**DAΦNE TECHNICAL NOTE**

INFN - LNF, Accelerator Division

Frascati, Nov.16, 1990

Note: **M-1**

# The DAΦNE SPLIT FIELD MAGNET

C. Sanelli

A preliminary design of the Split Field Magnet (SFM) for DAΦNE is described in this note.

The design parameters are:

| | | |
|---|---|---|
| Energy | 510 | MeV |
| Bending angle | 150 | mrad |
| Bending radius | 10 | m |
| Magnetic field | 0.17 | Tesla |
| Magnetic length | 1.5 | m |
| Entrance beam-beam separation | 10 | cm |
| Exit beam-beam separation | 32.46 | cm |
| Good field region ($\Delta B/B$ at ±25 mm) | $5\ 10^{-4}$ | |
| Full gap | 50 | mm |

An easy way to generate an alternate and compact magnetic field is to place, side by side, two H-type magnets with opposite polarity *(Fig.1-a)*. This arrangement can be further simplified by inspecting the magnetic flux path *(Fig.1-b)* in the central return leg, the fluxes from the two magnets cancel each other, and so no iron is necessary *(Fig.1-c)*.

The configuration shown in *Fig. 1-c* has been studied very carefully in two dimensions, by means of the computer code POISSON. We have focussed our attention to the entrance section which, due to the very tight beam's trajectory separation, is also the most critical one.

Different version of the adopted geometry have been investigated:

- version with iron poles and correction tips;
- version without tips but with correcting current wires near to the pole;
- window-frame version with different coil configurations.

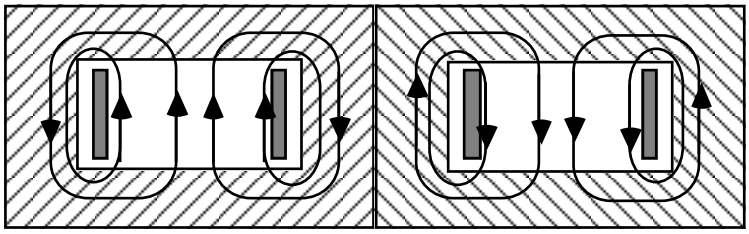

Fig. 1 a

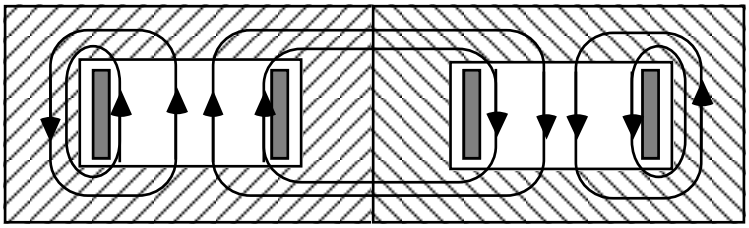

Fig. 1 b

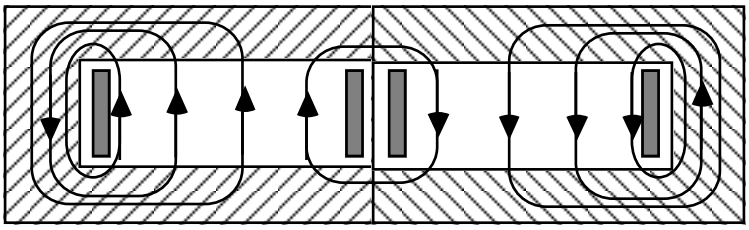

Fig. 1 c

**Fig. 1** - *Split field magnet rationale.*

We will discuss in the following just the last configuration since it is the more favourable from the field quality point of view.

Let us first discuss the 2-D calculations.

The geometry analysed with POISSON is schematically shown in *Fig. 2*. The horizontal coil size has been chosen, as small as possible, in order to improve the magnetic field homogeneity. The coil dimensions used in these calculations are $4.5 \cdot 4.5\ mm^2$.

*Fig. 3* shows the magnetic field lines. The mesh size used, in this POISSON run, is 1 mm in order to obtain better results.

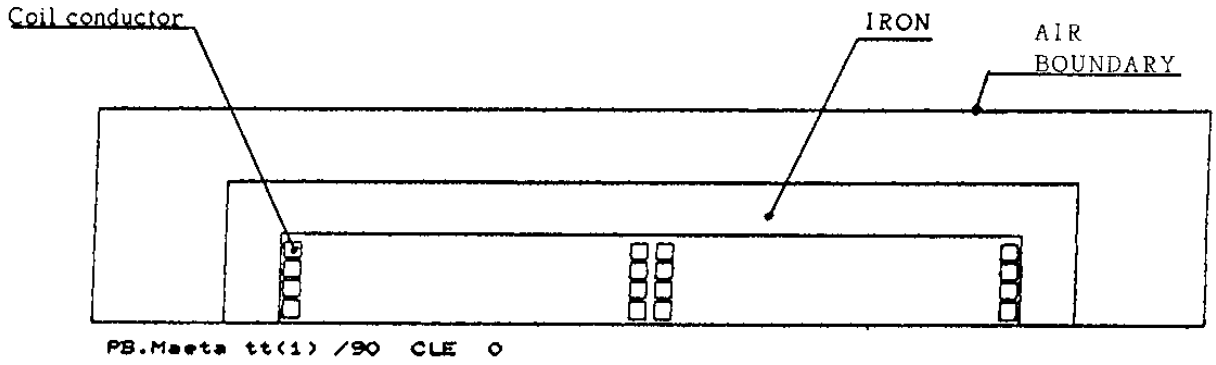


**Fig. 2** - *POISSON geometry.*

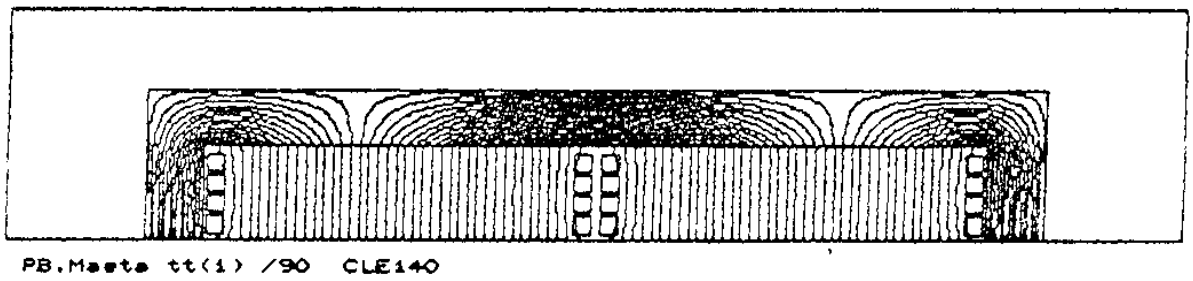


**Fig. 3** - *Field lines plotted by POISSON.*

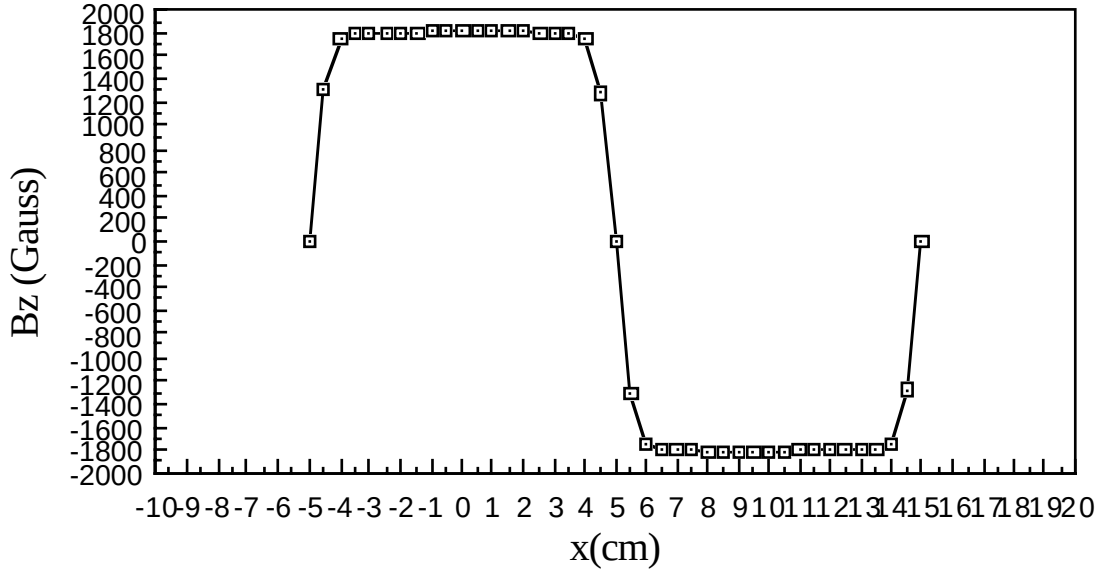


**Fig. 4** - $B_z(x)$ *(POISSON mesh 1 mm).*

*Fig. 4* shows the magnetic field, as calculated by POISSON, in the section under examination.

The maximum field deviation, with respect to the central one, is $\approx -7\ 10^{-4}$ at $x = 25$ mm. **Table I** lists the numerical values shown in *Fig. 4*. The x coordinate corresponds to the radial coordinate, perpendicular to the beam direction and laying on the horizontal plane. The beam centres are located at $x = 0.0$ mm and $x = 10.0$ mm respectively.

It is very important to underline the influence of the coil position into the magnet. Two cases, where the coil has been considered as a single turn having the same external dimensions of the four, have been investigated showing the effect of a 2 mm upward and downward shift on the field homogeneity. The Fig. 5 reports this effect. It is clear that during the magnet engineering design and manufacturing a lot of care must be put on the coil positioning in order to preserve the symmetry of the coil system.

A 3-dimensional calculation of the first 40 cm of magnet has been performed with the MAGNUS code. The plant and input views are given subsequently. The coil heads have been assumed saddle-type to leave more clearance for the vacuum pipe and to improve the fringing field quality. At this stage, elliptical vacuum chambers, one for each beam, have been considered. Fig. 6 shows the upper half of the iron with the four coils.

The resolution of the results is not so good (we have used nearly the maximum number of mesh points $\approx 14{,}000$ of the present version of MAGNUS) since the variations of the magnetic field take place on distances comparable to the mesh dimension, about 1 cm in the input section. Consequently the magnetic potential best fit done by the code cannot be very accurate giving an overshoot phenomenon with damped oscillations that can be clearly found on the table of the magnetic field values. Point by point results must be analysed very carefully, although the general field slopes confirm the POISSON results, taking into account the head fringe field effects that POISSON cannot evaluate.

The *figures 7, 8* and *9* show the magnetic field as function of the radial coordinate, $B_z(x)$, respectively at the beam entrance, in the middle of the magnet and at the magnet end. The high and narrow peaks correspond to the magnetic induction inside the iron return legs ($\approx 1.3$ Tesla).The flat-tops are the good field regions. It is evident how the useful zone, going from one section to the next, increases moving away from the interaction point.

*Fig. 10* shows some field lines on the central section of the magnet. MAGNUS displays some lines escaping from the iron. We will correct this effect by increasing the section of the return leg iron.

**TABLE I - 2-D magnetic fields vs. transverse coordinate.**

| | x (cm) | $B_z$ (Gauss) |
|---|---|---|
| 1 | -5.0 | 7.21 |
| 2 | -4.5 | 1302.50 |
| 3 | -4.0 | 1743.58 |
| 4 | -3.5 | 1797.98 |
| 5 | -3.0 | 1810.38 |
| 6 | -2.5 | 1813.66 |
| 7 | -2.0 | 1814.54 |
| 8 | -1.5 | 1814.76 |
| 9 | -1.0 | 1814.83 |
| 10 | -0.5 | 1814.88 |
| 11 | 0.0 | 1814.93 |
| 12 | 0.5 | 1815.01 |
| 13 | 1.0 | 1815.11 |
| 14 | 1.5 | 1815.18 |
| 15 | 2.0 | 1815.08 |
| 16 | 2.5 | 1814.33 |
| 17 | 3.0 | 1811.17 |
| 18 | 3.5 | 1798.86 |
| 19 | 4.0 | 1744.24 |
| 20 | 4.5 | 1294.57 |
| 21 | 5.0 | -0.9 |
| 22 | 5.5 | -1304.98 |
| 23 | 6.0 | -1744.28 |
| 24 | 6.5 | -1798.83 |
| 25 | 7.0 | -1811.16 |
| 26 | 7.5 | -1814.31 |
| 27 | 8.0 | -1815.06 |
| 28 | 8.5 | -1815.16 |
| 29 | 9.0 | -1815.08 |
| 30 | 9.5 | -1814.99 |
| 31 | 10.0 | -1814.91 |
| 32 | 10.5 | -1814.86 |
| 33 | 11.0 | -1814.80 |
| 34 | 11.5 | -1814.74 |
| 35 | 12.0 | -1814.51 |
| 36 | 12.5 | -1813.62 |
| 37 | 13.0 | -1810.34 |
| 38 | 13.5 | -1797.89 |
| 39 | 14.0 | -1743.11 |
| 40 | 14.5 | -1293.56 |
| 41 | 15.0 | -6.88 |

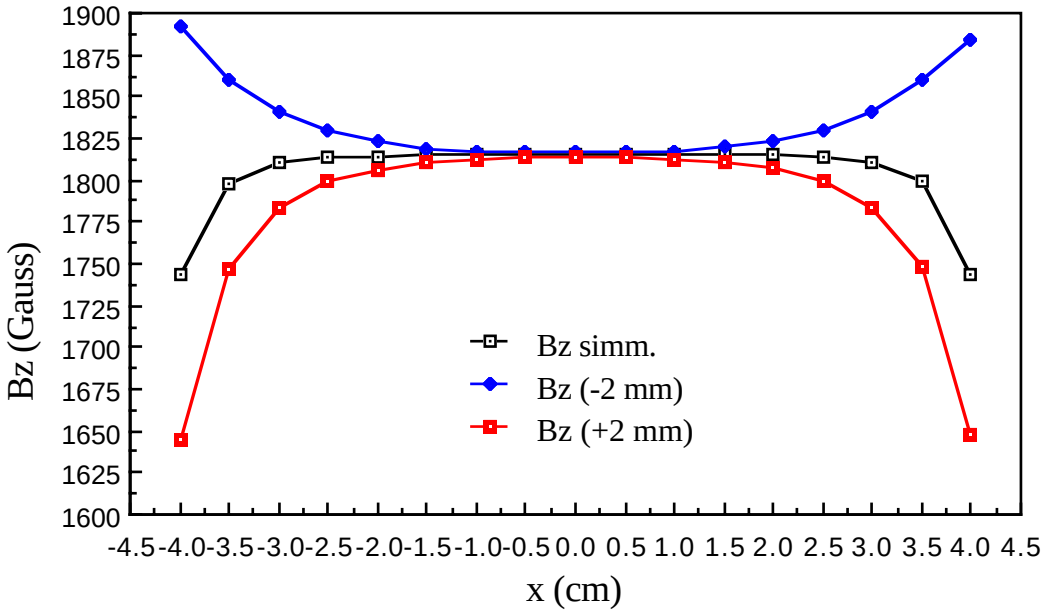


**Fig. 5** - $B_z(x)$ *as funcion of the coil position.*

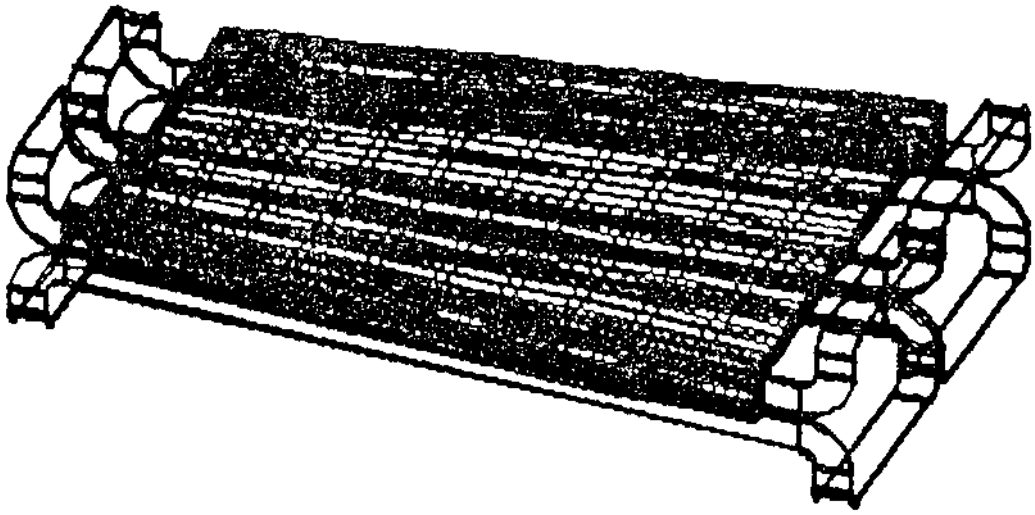

**Fig. 6** - *Upper half magnet with the coils.*

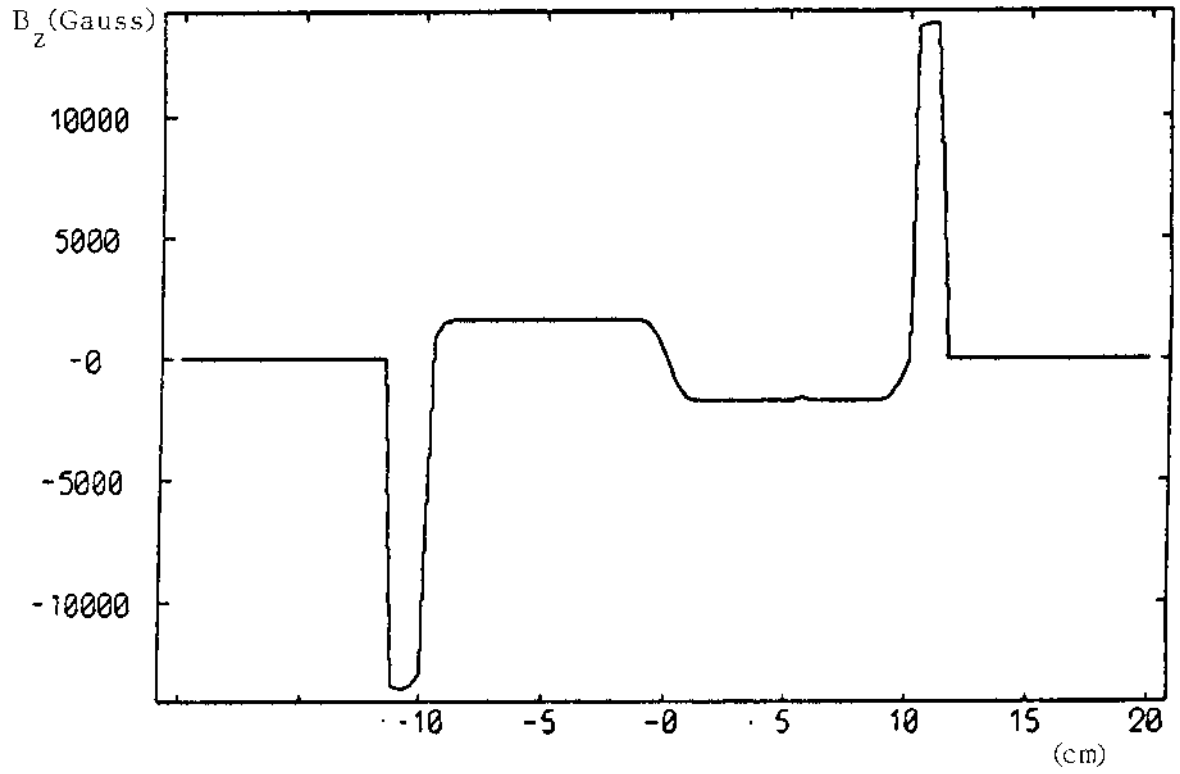


**Fig. 7** - $B_z(x)$ *at the beam entrance.*

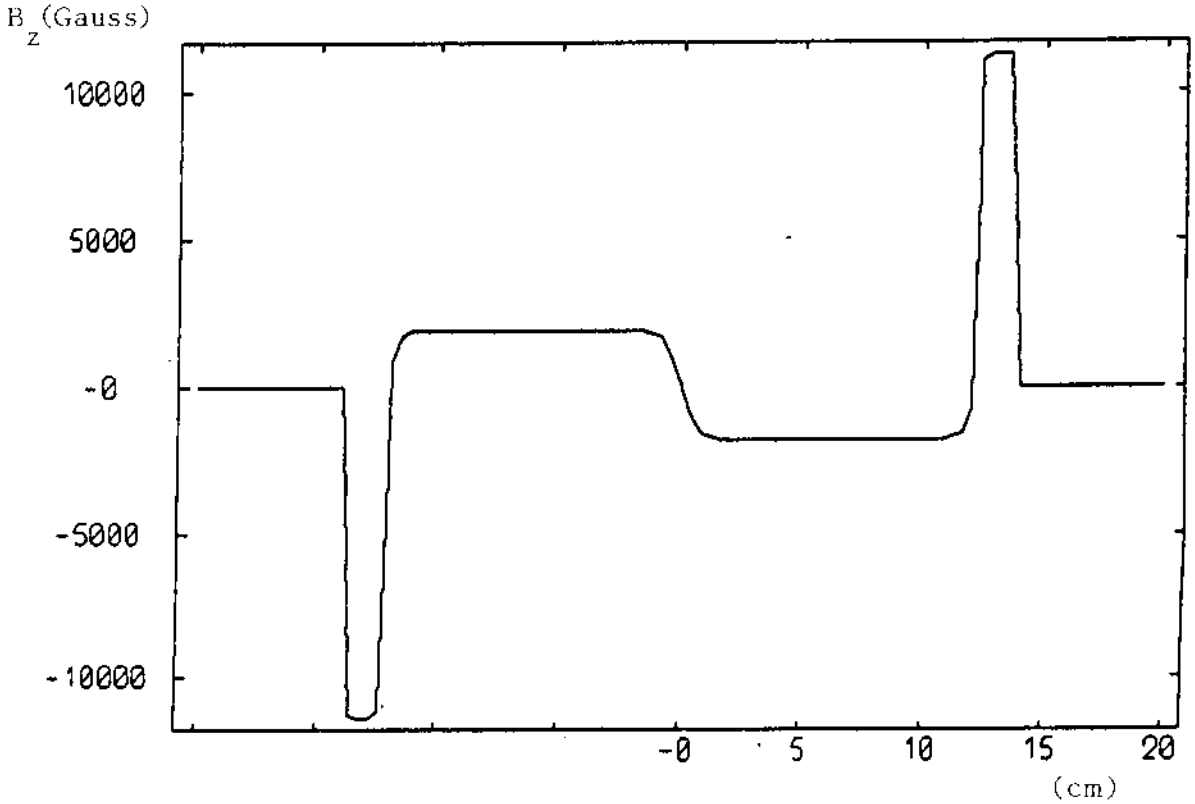


**Fig. 8** - $B_z(x)$ *at the center of the magnet.*

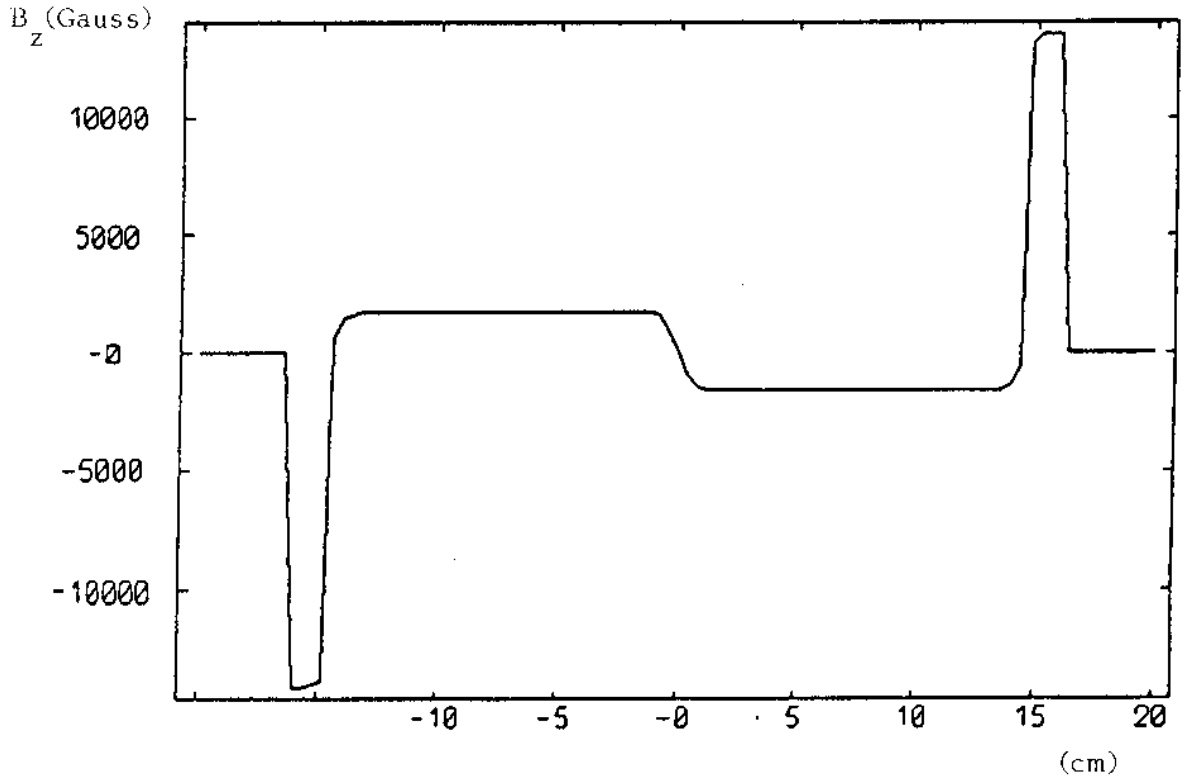


**Fig. 9** - $B_z(x)$ *at the beam exit.*

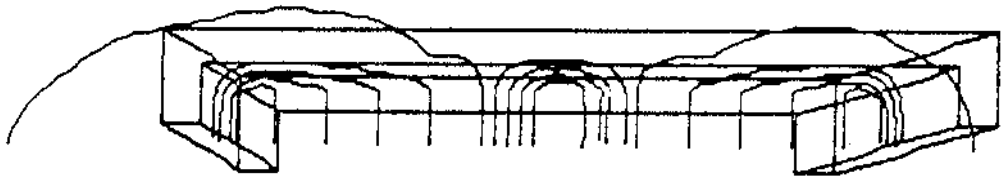

**Fig. 10** - *Field lines at the centre of the magnet.*

*Fig. 11* shows the results of POISSON and MAGNUS (200 against 20 mesh points are compared) at the magnet entrance. It is evident the field decreasing due to the head fringe field.

The MAGNUS predictions are not so good as POISSON for the already mentioned reasons, also if the field derivatives seem to be in good agreement in spite of the fast variations.

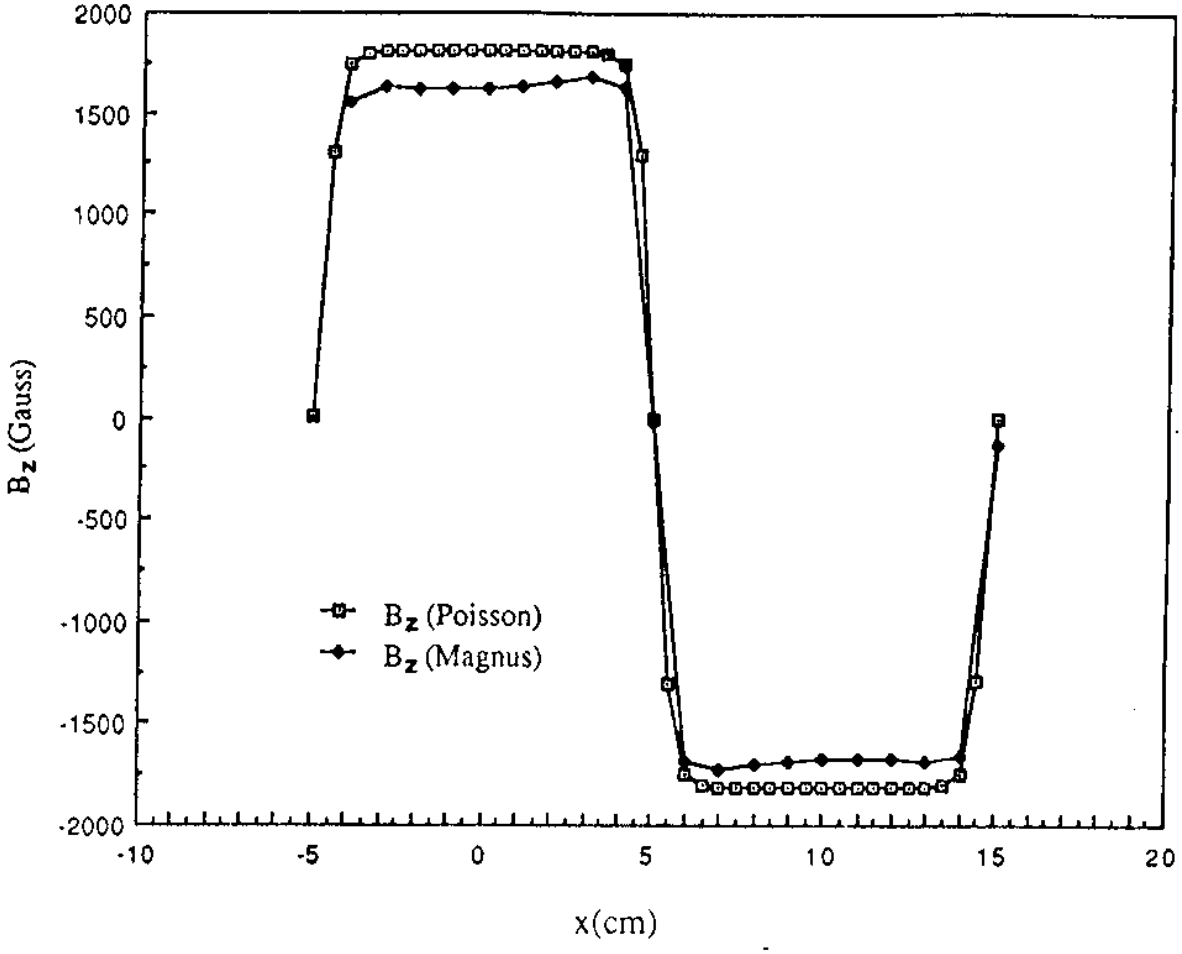


**Fig. 11** - *Magnetic field at the magnet entrance as evaluated by POISSON and MAGNET.*

*Fig. 12* shows the vertical component of the magnetic field $B_z(x)$ on different planes perpendicular to the beam direction, 5 cm far away each from the other, starting from the I.P. towards the magnet centre.

**Table II** lists the numerical values of *Fig. 12*.

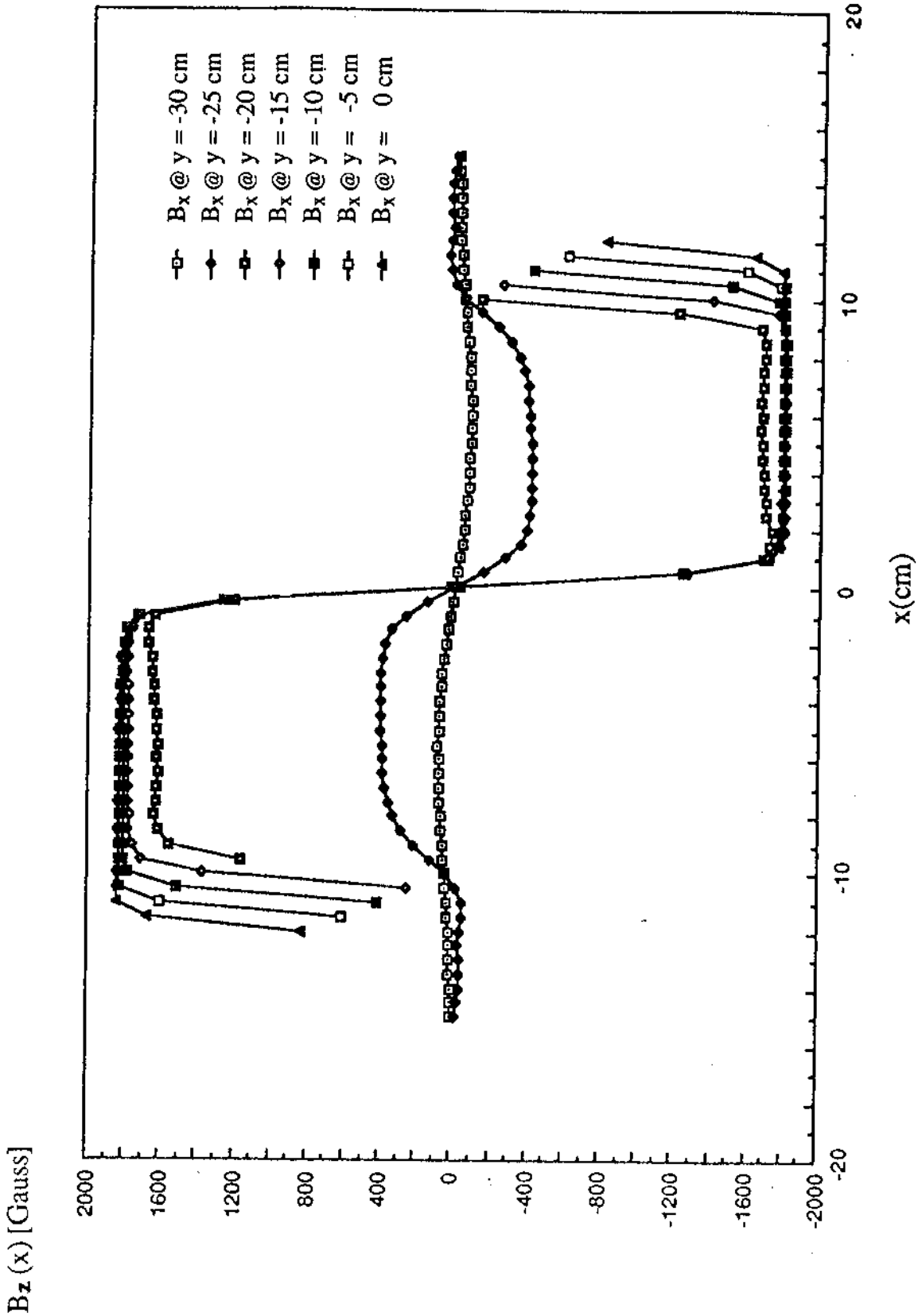


**Fig. 12** - *3-D magnetic field vs. radial coordinate at different longitudinal position.*

## TABLE II - *3-D* magnetic *field* (Gauss) *vs. radial coordinate* x *at different longitudinal* position y.

| | x (cm) | y=-30cm | y=-25cm | y=-20cm | y=-15cm | y=-10cm | y=-5cm | y=0cm |
|---|---|---|---|---|---|---|---|---|
| 1 | -15.0 | 2.0 | -17.6 | | | | | |
| 2 | -14.5 | 6.0 | -33.5 | | | | | |
| 3 | -14.0 | 10.5 | -39.7 | | | | | |
| 4 | -13.5 | 15.6 | -42.1 | | | | | |
| 5 | -13.0 | 17.0 | -40.9 | | | | | |
| 6 | -12.5 | 18.8 | -23.6 | | | | | |
| 7 | -12.0 | 21.1 | -39.7 | | | | | 831.5 |
| 8 | -11.5 | 25.5 | -52.3 | | | | 816.1 | 1670.4 |
| 9 | -11.0 | 30.5 | -47.0 | | | 418.4 | 1607.5 | 1840.2 |
| 10 | -10.5 | 36.1 | -15.7 | | 252.0 | 1511.5 | 1820.0 | 1838.0 |
| 11 | -10.0 | 42.3 | 40.5 | | 1370.4 | 1778.1 | 1826.0 | 1834.0 |
| 12 | -9.5 | 48.8 | 127.8 | 1157.4 | 1708.7 | 1797.6 | 1825.7 | 1827.8 |
| 13 | -9.0 | 55.2 | 219.6 | 1558.9 | 1750.5 | 1805.0 | 1820.2 | 1828.7 |
| 14 | -8.5 | 61.8 | 289.8 | 1611.1 | 1774.4 | 1800.7 | 1822.6 | 1833.5 |
| 15 | -8.0 | 67.4 | 333.6 | 1634.6 | 1772.2 | 1805.3 | 1824.6 | 1828.6 |
| 16 | -7.5 | 72.4 | 360.8 | 1623.3 | 1780.1 | 1804.5 | 1821.8 | 1832.0 |
| 17 | -7.0 | 76.6 | 374.7 | 1626.9 | 1776.9 | 1804.3 | 1826.1 | 1828.6 |
| 18 | -6.5 | 79.6 | 384.9 | 1617.0 | 1780.2 | 1805.6 | 1821.2 | 1828.5 |
| 19 | -6.0 | 81.3 | 391.6 | 1621.5 | 1778.5 | 1803.7 | 1824.2 | 1829.8 |
| 20 | -5.5 | 81.8 | 396.1 | 1615.8 | 1780.5 | 1807.5 | 1821.1 | 1826.5 |
| 21 | -5.0 | 80.8 | 401.3 | 1623.4 | 1780.1 | 1803.5 | 1821.8 | 1831.3 |
| 22 | -4.5 | 78.1 | 402.6 | 1621.2 | 1781.7 | 1809.8 | 1822.2 | 1825.0 |
| 23 | -4.0 | 74.4 | 404.7 | 1634.0 | 1782.5 | 1803.1 | 1818.7 | 1826.4 |
| 24 | -3.5 | 69.0 | 404.8 | 1634.1 | 1782.5 | 1808.3 | 1826.7 | 1825.6 |
| 25 | -3.0 | 62.0 | 401.7 | 1653.9 | 1784.9 | 1801.4 | 1813.0 | 1817.4 |
| 26 | -2.5 | 54.0 | 394.8 | 1654.4 | 1779.4 | 1801.5 | 1818.2 | 1827.9 |
| 27 | -2.0 | 44.5 | 375.9 | 1679.3 | 1782.1 | 1795.8 | 1803.5 | 1804.2 |
| 28 | -1.5 | 33.8 | 338.2 | 1669.7 | 1757.3 | 1774.9 | 1786.1 | 1790.9 |
| 29 | -1.0 | 22.8 | 266.4 | 1639.4 | 1703.0 | 1718.2 | 1726.1 | 1727.9 |
| 30 | -0.5 | 10.6 | 148.3 | 1204.5 | 1243.6 | 1259.3 | 1267.7 | 1270.7 |
| 31 | 0.0 | -1.8 | -6.2 | -23.9 | -11.1 | 4.9 | 13.7 | 17.9 |
| 32 | 0.5 | -14.1 | -160.7 | -1252.4 | -1265.9 | -1249.4 | -1240.4 | -1235.0 |
| 33 | 1.0 | -26.1 | -278.8 | -1687.3 | -1725.3 | -1708.3 | -1698.8 | -1692.1 |
| 34 | 1.5 | -37.3 | -350.6 | -1717.6 | -1779.8 | -1765.0 | -1758.7 | -1755.2 |
| 35 | 2.0 | -48.0 | -388.3 | -1727.1 | -1804.4 | -1785.9 | -1776.2 | -1768.4 |
| 36 | 2.5 | -57.4 | -407.0 | -1702.3 | -1801.7 | -1791.6 | -1790.8 | -1792.2 |
| 37 | 3.0 | -65.4 | -413.9 | -1701.8 | -1807.2 | -1791.5 | -1785.7 | -1781.7 |
| 38 | 3.5 | -72.4 | -416.9 | -1681.9 | -1804.9 | -1798.4 | -1799.4 | -1789.8 |
| 39 | 4.0 | -77.8 | -416.6 | -1681.8 | -1804.8 | -1793.2 | -1791.4 | -1790.6 |
| 40 | 4.5 | -81.4 | -414.4 | -1669.0 | -1804.0 | -1799.9 | -1794.8 | -1789.3 |
| 41 | 5.0 | -84.0 | -413.0 | -1671.3 | -1802.5 | -1793.6 | -1794.4 | -1795.5 |
| 42 | 5.5 | -85.0 | -407.6 | -1663.8 | -1802.9 | -1797.6 | -1793.7 | -1790.7 |
| 43 | 6.0 | -84.4 | -403.0 | -1669.6 | -1801.0 | -1793.8 | -1796.8 | -1794.0 |
| 44 | 6.5 | -82.6 | -396.1 | -1665.6 | -1802.9 | -1795.7 | -1793.7 | -1792.7 |
| 45 | 7.0 | -79.8 | -385.7 | -1676.6 | -1799.9 | -1794.3 | -1798.6 | -1792.7 |
| 46 | 7.5 | -75.4 | -371.6 | -1675.4 | -1803.6 | -1794.4 | -1794.1 | -1796.0 |
| 47 | 8.0 | -70.3 | -344.3 | -1689.1 | -1796.7 | -1795.0 | -1796.6 | -1792.3 |
| 48 | 8.5 | -64.4 | -300.4 | -1688.6 | -1800.6 | -1790.2 | -1794.2 | -1797.0 |
| 49 | 9.0 | -57.9 | -230.3 | -1659.5 | -1786.0 | -1793.8 | -1791.1 | -1791.6 |
| 50 | 9.5 | -51.4 | -136.5 | -1207.6 | -1751.6 | -1782.6 | -1794.3 | -1790.1 |
| 51 | 10.0 | -44.7 | -51.1 | -135.0 | -1395.3 | -1759.4 | -1785.3 | -1792.8 |
| 52 | 10.5 | -38.3 | 3.7 | | -255.5 | -1500.2 | -1770.0 | -1785.8 |
| 53 | 11.0 | -32.5 | 33.9 | | | -413.6 | -1575.0 | -1776.9 |
| 54 | 11.5 | -27.3 | 41.1 | | | | -605.5 | -1626.6 |
| 55 | 12.0 | -22.7 | 33.2 | | | | | -814.2 |
| 56 | 12.5 | -20.1 | 21.6 | | | | | |
| 57 | 13.0 | -17.9 | 31.5 | | | | | |
| 58 | 13.5 | -16.2 | 29.3 | | | | | |
| 59 | 14.0 | -12.2 | 23.4 | | | | | |
| 60 | 14.5 | -8.7 | 16.4 | | | | | |
| 61 | 15.0 | -5.6 | 8.7 | | | | | |

*Fig. 13* shows $B_z(y)$ as function of the ideal beam trajectory.

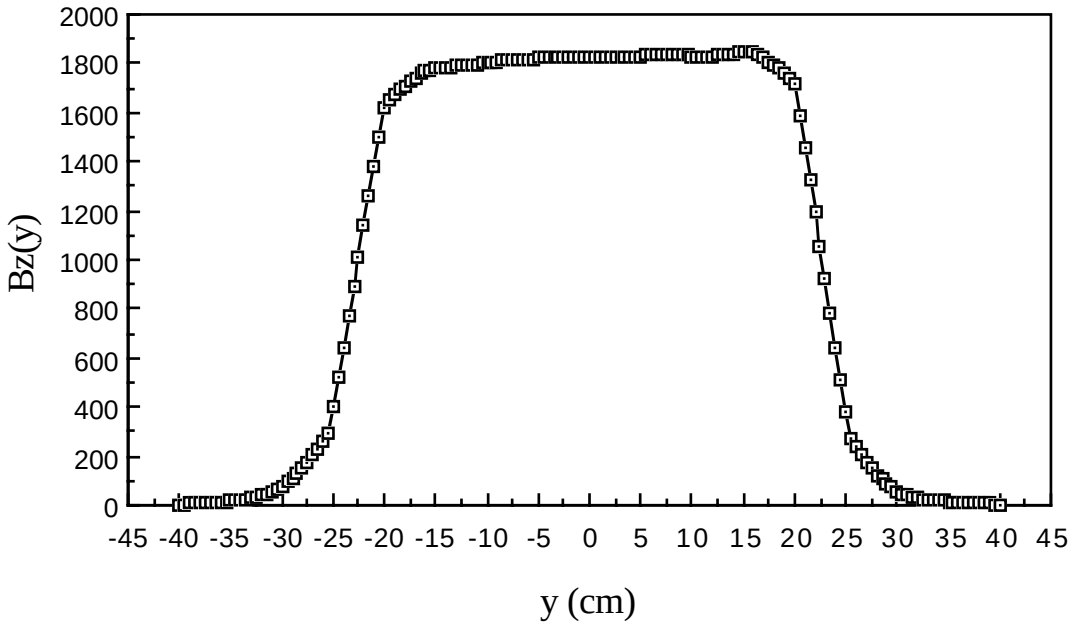


**Fig. 13** - $B_z$ *along beam trajectory*.

*Fig. 14* shows the magnet input section, scale 1:1, adopted in the electromagnetic calculations.

*Fig. 15* shows a plant view of the magnet whose first 40 cm have been investigated with the 3D code.

## CONCLUSIONS

The previous results indicate that it is judicious to realize a prototype. So doing, we can measure the fringing which are difficult to calculate, and check the effectiveness of the engineering solutions.

In our opinion a magnet with the same transverse section, scale 1:1 and 40 cm long (≈ 8 gaps) is adequate.

In the following we give the electric and hydraulic parameters for this prototype as well for the final magnet.

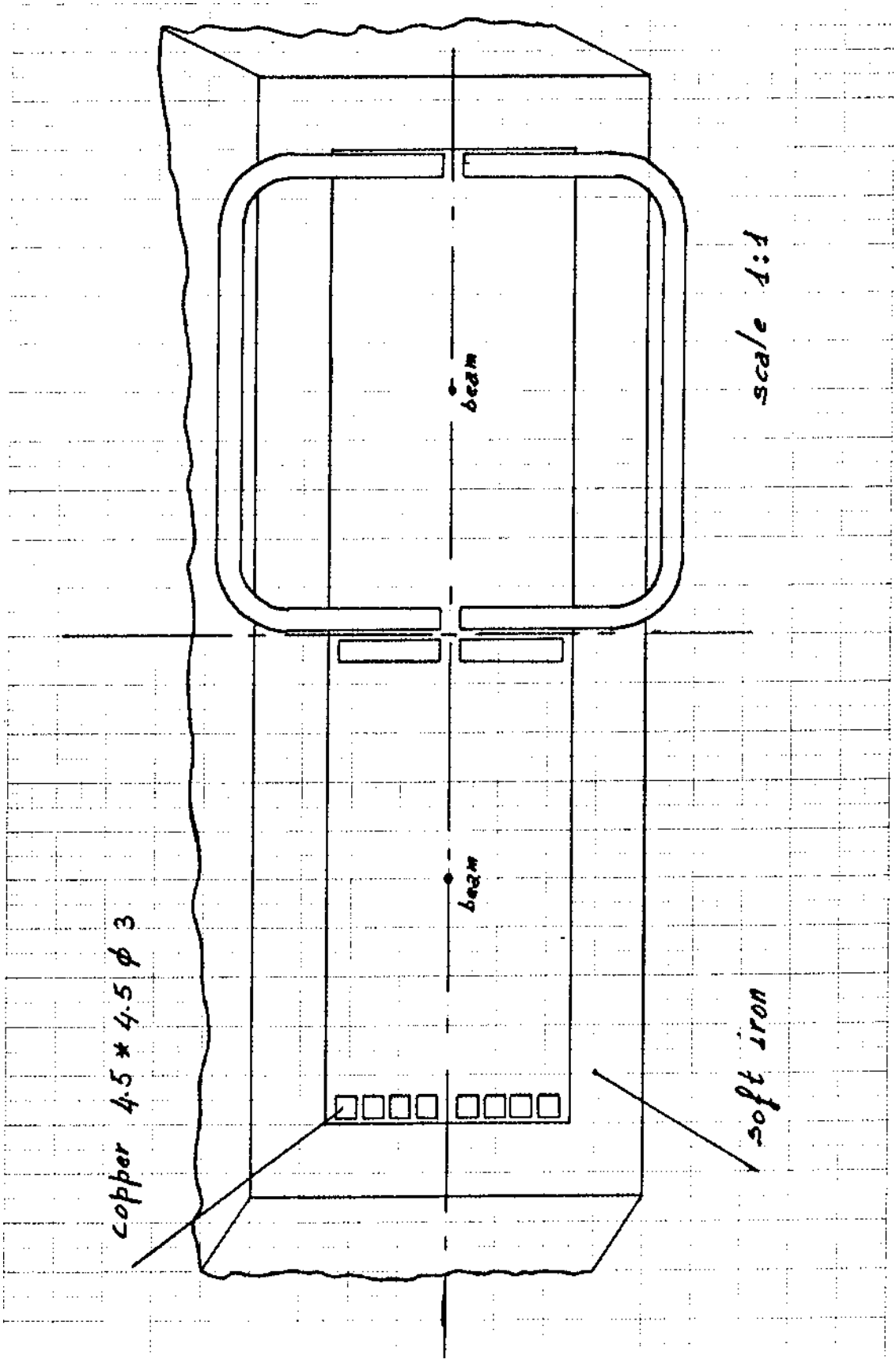


**Fig. 14** - *Front view at the input section.*

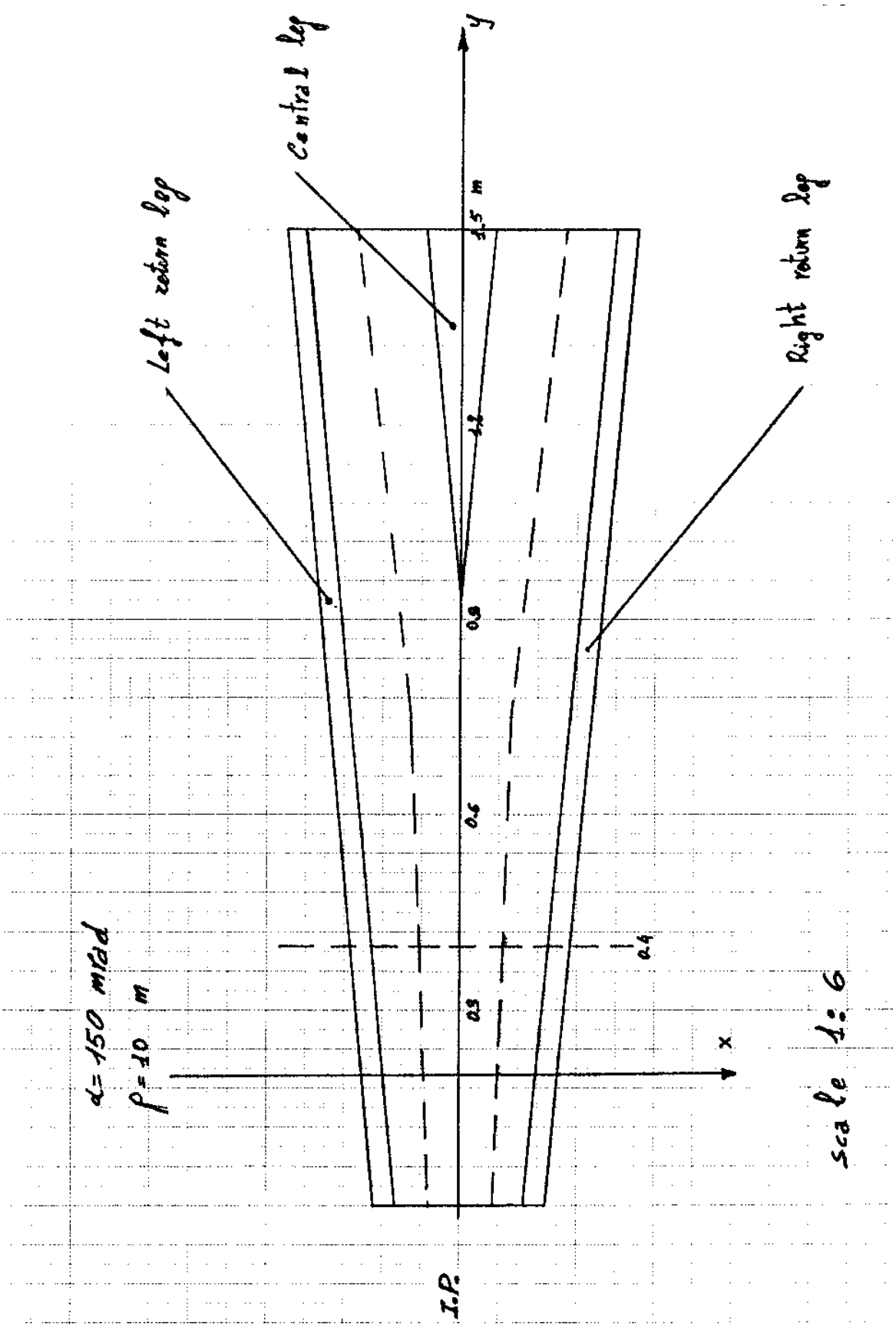


**Fig. 15** - *Plant view of the Split-field magnet.*

## Electrical and hydraulic parameters

Each coil has 4 turns that are in series for electrical connections and in parallel for hydraulic connections. The two right side coils, as the two on the left, will be electrically in series. It is not sure, at the moment if it will be used only one or two power supplies to compensate little differences of the magnetic field flat-tops.

The data that follows refer to the series of all the four coils.

*Electrical parameters*

| | Prototype | Final | |
|---|---|---|---|
| Conductor Cu | 4.5 4.5 Ø 3 | 4.5 4.5 Ø 3 | |
| Average turn length | 1.8 | 4.1 | m |
| Conductor length /coil | 7.2 | 16.4 | m |
| Coil resistance(60 °C) | 11 | 25 | mΩ |
| Total resistance | 44 | 100 | mΩ |
| Nominal current | 845.8 | 845.8 | A |
| Current density | 64.2 | 64.2 | $A/mm^2$ |
| Total voltage | 37.2 | 84.6 | V |
| Total power | 31.5 | 71.5 | kW |

*Hydraulic parameters* (16 circuits in parallel)

| | Prototype | Final | |
|---|---|---|---|
| Average turn length | 1.8 | 4.1 | m |
| Power to dissipate for circuit | 1968 | 4478 | W |
| Water flow ($\Delta T = 30$ ° C) | $1.56\ 10^{-5}$ | $3.55\ 10^{-5}$ | $m^3/sec$ |
| $H_2O$ velocity | 2.21 | 5.03 | m/sec |
| N° Reynolds | 14486 | 32961 | |
| Pressure drop | 0.43 | 4.13 | Ate |

The conductor dimensions can probably be optimized from the hydraulic point of view to have the possibility to reach an energy of about 750 MeV. Studies on this direction are under investigation.